ACS NANO
Cite This: ACS Nano 2018, 12, 6784−6793
www.acsnano.org

ARTICLE

Synthesis of Highly Uniform Nickel Multipods with Tunable Aspect Ratio by Microwave Power Control

Parth N. Vakil, David A. Hardy, and Geoffrey F. Strouse*

Department of Chemistry and Biochemistry, Florida State University, Tallahassee, Florida 32306-4390, United States

Supporting Information

ABSTRACT: As the importance of anisotropic nanostructures and the role of surfaces continues to rise in applications including catalysis, magneto-optics, and electromagnetic interference shielding, there is a need for efficient and economical synthesis routes for such nanostructures. The article describes the application of cycled microwave power for the rapid synthesis of highly branched pure-phase face-centered cubic crystalline nickel multipod nanostructures with >99% multipod population. By controlling the power delivery to the reaction mixture through cycling, superior control is achieved over the growth kinetics of the metallic nanostructures, allowing formation of multipods consisting of arms with different aspect ratios. The multipod structures are formed under ambient conditions in a simple reaction system composed of nickel acetylacetonate ($Ni(acac)_2$), oleylamine (OAm), and oleic acid (OAc) in a matter of minutes by selective heating at the (111) overgrowth corners on Ni nanoseeds. The selective heating at the corners leads to accelerated autocatalytic growth along the ⟨111⟩ direction through a "lightning rod" effect. The length is proprtional to the length and number of microwave (MW)-on cycles, whereas the core size is controlled by continuous MW power delivery. The roles of heating mode (cycling *versus* variable power *versus* convective heating) during synthesis of the materials is explored, allowing a mechanism into how cycled microwave energy may allow fast multipod evolution to be proposed.

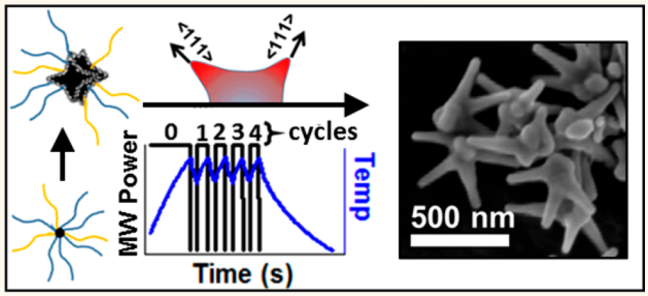

KEYWORDS: *nickel, multipod, anisotropic, microwave, nanoparticle, mechanism, lightning rod effect*

The growth of metal nanoparticles is known to follow an autocatalytic two-step Finke−Watzky mechanism, where the first step involves a slow reduction step (k_1) of the cationic precursor in solution by a weak reducing agent, such as oleylamine, followed by a second fast reduction step (k_2) of the cation precursor at the surface of the growing nanoparticle.[1−3] In the autocatalytic mechanism, $k_2 \gg k_1$, leading to growth being dominated by the nanoparticle surface. The nuclei morphology, the facet stability for a given metal, the reaction conditions, and face-selective binding of ligands can lead to hyper-branching. Although spherical particles are no doubt important materials, controlling the reaction to allow isolation of high surface area branched metal nanoparticles is attractive for catalysis and plasmonic applications.[4−13]

Recent studies have revealed for face-centered cubic (fcc) metals that branching is achieved by initial overgrowth on the high-energy vertex and edge sites corresponding to the (111) facets. Xia *et al.* revealed that morphology control can be achieved by preferential growth along the (111) facet initiated by (111) overgrowth occurring on nucleated cubic (fcc) nanometal seeds.[5] Researchers have carried the overgrowth ideas to other metals and shown that materials with rapid metal reorganization lead to primarily isotropic structures (Au, Ag, Cu), whereas structures with slow reorganization can readily grow as anisotropic structures (Ni, Pd, Pt).[14,15] The breakthrough in understanding the mechanism results in routes to achieve the desired morphology. For catalytic applications, multipod Ni, Pt, and Pd nanoparticles have been reported, although the systematic control of arm length and aspect ratio is poor, and long reaction times limit the scalability of the reactions.[16−21] To truly realize the benefits of multipod nanostructured materials, it is critical to develop simple, economical, scalable, reliable, and efficient routes for their synthesis.

Transitioning the mechanistic understanding of growth to sustainable synthetic methods for solution-processed materials, whether by flow chemistry, batch reactors, or, more recently, microwave-assisted methods, is fundamentally important as such materials are being used for catalytic and plasmonic

Received: March 16, 2018
Accepted: June 18, 2018
Published: June 18, 2018

DOI: 10.1021/acsnano.8b01992
ACS Nano 2018, 12, 6784−6793

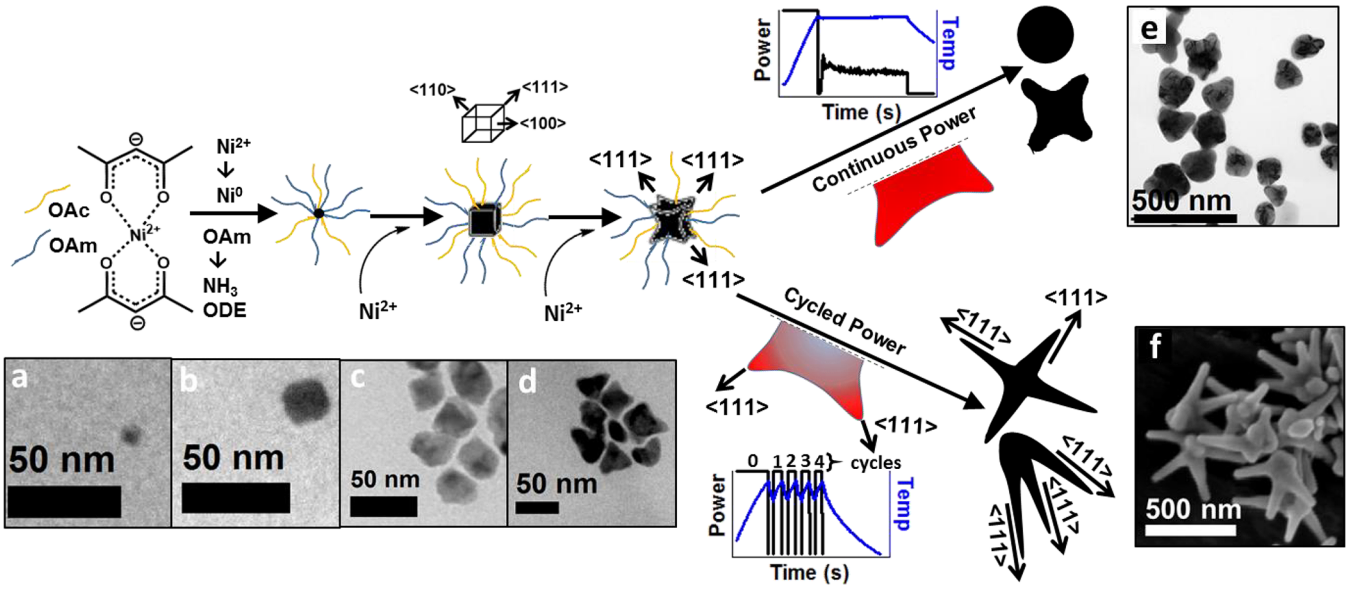

Figure 1. Proposed mechanism of nickel multipod growth during cycled microwave heating. The growth of Ni occurs *via* a two-step autocatalytic process, where $Ni(acac)_2$ is reduced in solution by the weak reducing agent, oleylamine, followed by the formation of small nickel nuclei capped by oleylamine and oleic acid that continue to grow. The rates of growth are controlled by facet energy, with the (111) facet being energetically favored. During the microwave "on" cycle, selective heating of (111) tips on nanoparticle corners enables faster autocatalytic growth. Fastest growth of long multipod arms is therefore enabled when using high microwave power cycles that provide a greater differential temperature between arm tips and the rest of the nanoparticle surface, unlike the case of the continuous power mode, where particle reaches thermal equilibrium.

applications.[22,23] In the past decade, the use of microwave (MW) chemistry for nanomaterial synthesis has attracted attention due to the enhancement of reaction rates and reproducibility of the materials when carried out in a single-mode MW reactor. The observed enhancement is not due to the energy absorbed per MW photon, as it does not contain enough energy to break a bond, but rather to enhanced growth rates reflecting the evolving dielectric loss tangent for the growing nanoparticle. The size-dependent loss tangent reflects the repolarization of the electric field, as described within the Maxwell–Wagner (M–W) model.[24] Such polarization effects are anticipated to be enhanced at sharp tips and edges, leading to enhanced heating at these sites in a growing metal. This is referred to as a "lightning rod" effect because the sharp tips and edges generate very high electric fields in their vicinity due to the surface charge density in those regions.[25−32] The size- and shape-dependent M–W loss tangents for a metal nanoparticle suggest that selective heating of the tip under cycled power may provide control through selective tip growth acceleration. MW power cycling as a tool in MW chemistry has been suggested by organic chemists to enhance yield of reactions and in materials synthesis to manipulate heating rates. Although the fundamental physics are well understood and the lightning rod effect has been shown to enhance electromagnetic shielding,[28,31,33−35] the use in MW synthesis has not been explored.

In this work, we show a simple and rapid microwave-assisted chemical reaction that takes minutes to produce highly crystalline metallic fcc nickel multipod structures. Nickel is chosen as the example material as it is a highly valuable industrial catalyst in fuel cells, waste reduction, and bioprocessing technologies.[36−41] Ni multipods with arms that are 230 nm in length and 51 nm in width (aspect ratio of 4.5) can be routinely prepared by sequential MW power cycling (nine cycles) in a 2.45 GHz MW single-mode cavity (300 W) within 10 min. The application of single-mode cycled MW heating is demonstrated to enhance growth of the (111) facet to form multipod Ni nanoparticles with large aspect ratios. The arm length of the Ni multipod is easily controlled by the number and time of cycles applied during growth. This method does not need inert conditions to produce particles. The aspect ratio is systematically reduced with fewer cycles. The resulting multipod structures are highly crystalline metallic single-phase fcc nickel. The high aspect ratio samples are not achieved by continuous MW operation.

It is hypothesized that the ability to generate multipod structures selectively reflects local tip heating, leading to acceleration of the (111) facet growth on the initial Ni seed crystal. As the arm grows, the selective heating coupled to an increased MW cross section for the anisotropic structure results in the observed >99% selective multipod formation. Mechanistically, the accelerated growth is describable under the Finke–Watzky autocatalytic mechanism as a temperature-enhanced growth rate on the (111) facet, which occurs faster than atom reorganization on the seed faces. The lack of multipod formation under continuous power is ascribed to the fact that the system reaches equilibrium, and the growth of the (111) facet is in competition with nanocrystal reconstruction to minimize surface energy.

The study furthers the demonstration of microwave-driven chemistry as a powerful technology, providing precise control over nanomaterial growth and morphology, with lower energy consumption.[42−44] Although multipod structures can be achieved in classical convective reactions by addition of ligands that selectively bind to a facet, the use of the cycled MW produces >99% multipod morphology.

RESULTS AND DISCUSSION

Although Ni nanoparticle growth is well understood, controlling morphology is not as predictable with typical

DOI: 10.1021/acsnano.8b01992
ACS Nano 2018, 12, 6784–6793

reactions, yielding a distribution of morphologies.[18,20,45] In all reactions, enhancing growth at the tips (overgrowths) is key to achieving the desired selective control of (111) growth, allowing larger reaction batches to be prepared in isolating anisotropic morphologies. Enhancing tip growth requires control of surface energy, which can be achieved by ligand binding or potentially selective heating. MW heating can give rise to selective heating due to the fact that MW absorption by a nanoparticle is size- and shape-dependent.[2,24,46] The interaction of the MW field will be largest at sharp edges, reflecting the properties of the dielectric absorption process.[28,31,33−35] In systems exhibiting overgrowth, this may lead to selective heating of the tips and potentially increased reduction rates at the overgrowth sites owing to the lightning rod effect,[25−32] leading to enhanced anisotropic growth at the superheated tips as hypothesized in Figure 1. Of course, under continuous MW absorption, as the nanoparticle reaches thermal equilibrium, this effect will be diminished, leading to the reported spherical shapes.

The degree of experimental control achieved by MW power cycling *versus* continuous MW power is illustrated in selected electron microscopy images showing initial nucleation and growth results in cubic structures (Figure 1a−c) that evolve toward (111) overgrowth (Figure 1d) maintained under continuous power (Figure 1e) but lead to high aspect ratio multipod morphologies under cycled conditions (Figure 1f). As detailed below, the evolution from cubic to overgrowth to high aspect ratio multipods was analyzed as a function of time (number of cycles) to produce a mechanism for growth that distinguishes autocatalytic growth observed in MW reactors for Ni under continuous heating from the onset of MW-enhanced (111) facet growth under cycled MW conditions. To evaluate the effect of MW power cycling on anisotropic growth, the nanoparticles were grown by one of two operational modes: (1) constant temperature mode (280 °C) (instrument maintains temperature with adjusting the power automatically) and (2) power- and frequency-dependent cycling of MW power. Comparison to heating in a convective reaction using a round-bottom flask and aluminum block was carried out to evaluate the proposed growth model.

Condition 1: Evolution of Multipods under Constant Temperature Mode for MW Heating (Variable Power). The influence of time on multipod formation was evaluated under constant temperature conditions where the MW power fluctuates to maintain temperature over the course of the reaction. The reactions were carried out by heating a solution of $Ni(acac)_2$ dissolved in a 5:1 (v/v) ratio of oleylamine to oleic acid to 280 °C using an initial incident power of 300 W to reach 280 °C and allowing the power to fluctuate to maintain the reaction temperature (see Figure 1 for the continuous power graphic). The reaction temperature and microwave power profile for a continuous temperature reaction and resulting particles are shown in Figure 2A−H. Comparison is made to a reaction where the power is decreased from 300 to 75 W under controlled power, as a direct comparison to the constant temperature study.

During the Ni growth reaction under constant temperature conditions, the power cycles after 2 min decreased from 300 to 0 W, with continuous power fluctuation at ∼50−100 W to maintain reaction temperature. Small power fluctuations are evident in the constant temperature reaction. In contrast, under constant power (Figure 2J), the temperature is maintained over the course of the reaction without power fluctuations.

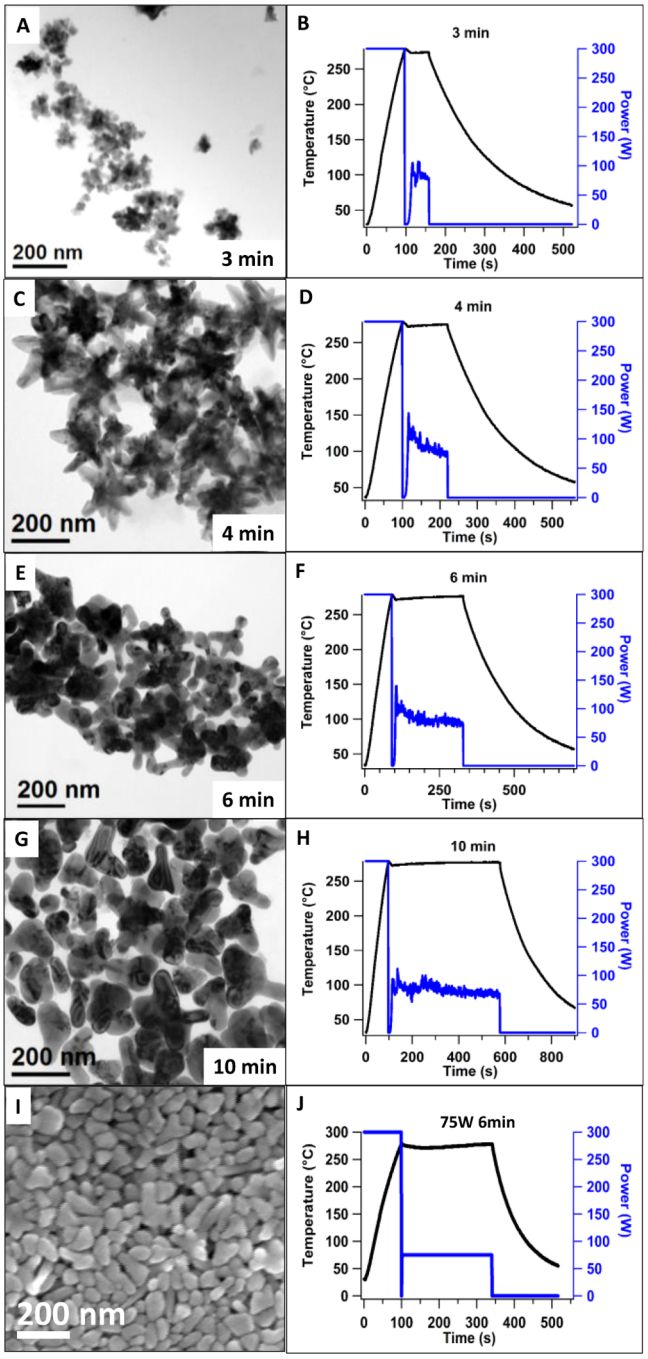

Figure 2. Transmission electron microscopy images of nickel multipods under constant temperature mode at different times of (A) 3 min, (C) 4 min, (E) 6 min, and (G) 10 min. Temperature and microwave power profiles for the (B) 3 min, (D) 4 min, (F) 6 min, and (H) 10 min reactions. Scanning electron microscopy images of nickel multipods under constant power mode for (I) 6 min and (J) corresponding temperature and microwave power profile.

In Figure 2, no clear correlation is observed between the length of reaction at 280 °C (constant temperature) and the appearance of multipod arms. Reactions carried out for 3 min (1 min beyond cycle event) during the largest variance in power produce irregularly shaped nanoparticles exhibiting overgrowth but wide dispersities in size (20−100 nm). After 4

DOI: 10.1021/acsnano.8b01992
ACS Nano 2018, 12, 6784−6793

min (2 min beyond cycle event), the nanoparticles have grown larger and exhibit clear multipod morphology (arm aspect ratio of 1.4) with tapering arms. From 6 to 10 min, the particles exhibit variability in the multipod morphology, having large sphere-like cores with longer arms of uniform width and rounded ends extending out from the core (arm aspect ratio of 1.6−1.4). The stepped power experiment produces nonuniform shaped Ni (Figure 2I) consistent with the 6−10 min reactions.

The average arm length, arm width, and aspect ratio for each time point are provided in Table 1, and distributions extracted from the transmission electron microscopy (TEM) images are provided in Supporting Information Figure SF1. Arm length is reported as the length from tip to base of the arm, and width is measured across the center region of the multipod arm.

Table 1. Multipod Arm Length, Width, And Aspect Ratio with Respective Standard Deviations for Various Reactions Using Constant Temperature Mode Related to Figure 2[a]

reaction	arm length (nm)	arm length standard deviation (nm)	arm width (nm)	arm width standard deviation (nm)	aspect ratio	aspect ratio relative standard deviation
3 min	16	7.5	14	5.1	1.1	0.59
4 min	55	19	38	10	1.4	0.44
6 min	77	26	50	13	1.6	0.43
10 min	81	31	58	10	1.4	0.42

[a]The reaction for constant power mode (75 W, 6 min) produces sphere-like nanoparticles with a diameter of 72 ± 12 nm.

The 4 and 10 min Ni nanocrystals were investigated by high-resolution TEM (HRTEM) lattice spacing analysis to assess the crystallinity (Supporting Information Figure SF2A,B). A HRTEM image of the arms in the 4 min reaction shows the arms grow along the ⟨111⟩ direction with a *d*-spacing of 0.20 nm with no visible glide plane errors. In the 10 min reaction, the overgrowths on the 10 min Ni nanoparticle also conform to the (111) plane with a *d*-spacing of 0.20 nm. Powder X-ray diffraction (pXRD) patterns on the 10 min reaction confirm the *d*-spacing assignments to fcc Ni (Supporting Information Figure SF3).

The lack of a clear power or time dependence on growth behavior using constant temperature is attributed to the large fluctuation in the MW power cycle profiles. To assess the effect of MW influence, controlled convective reactions were carried out under reaction conditions identical to those of the constant temperature studies in Figure 2 (280 °C, 5:1 OAm:OAc, 0.08 M $Ni(acac)_2$) for 4 min in a preheated aluminum block and 1 h using a round-bottom flask with a heating mantle. In the convective reactions, the NiNPs appear as spherical nanocrystals (Supporting Information Figure SF4). The formation of overgrowth and multipod arms is not observed under convective conditions despite using a fast ramp rate using an aluminum block to mimic microwave ramp rates. The lack of overgrowth under the experimental conditions is consistent with reports where high-temperature reactions lead to spherical nanocrystals.[15,45,47,48]

The shapes of the NiNPs grown under convective conditions compared to NiNPs grown in a MW are different. It is clear in Figure 2 that the NiNPs grown in a MW exhibit overgrowth leading to multipod structures. Inspection of the power *versus* time graphs suggests the multipod formation in the MW is potentially due to the presence of MW power cycling.

Evolution of Multipods under Cycled Microwave Power (Variable Temperature and Reaction Time). The influence of MW power cycling on multipod formation was evaluated under variable temperature and time to evaluate whether cycling of the impingent MW field (Figure 3) directly correlated to the length of the arm observed in the MW reactions (Figure 4). The cycle power and temperature profiles for the experimental conditions that produce the multipod structures in Figure 4 are shown in Figure 3.

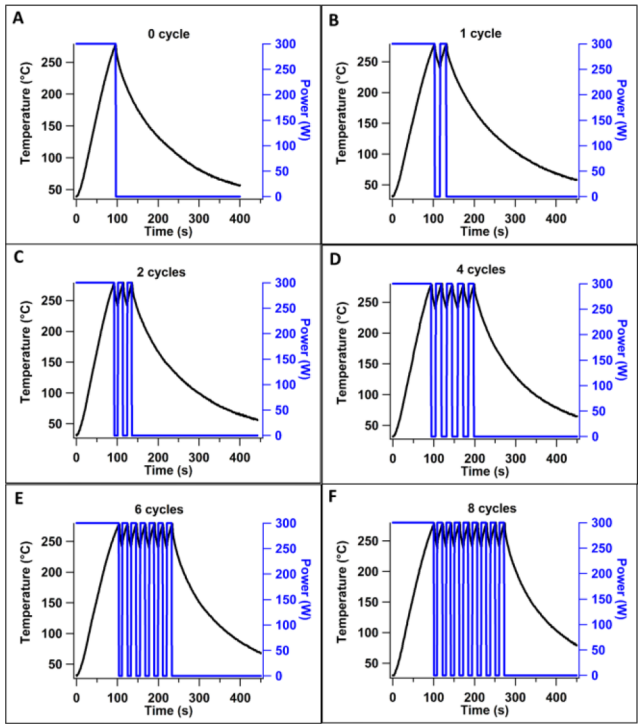

Figure 3. Temperature and power profiles for cycled power mode microwave reactions with (A) 0 cycle, (B) 1 cycle, (C) 2 cycles, (D) 4 cycles, (E) 6 cycles, and (F) 8 cycles.

The reactions are carried out under reaction conditions identical to those of the constant temperature study; however, the MW is cycled using 300 W in a controlled fashion, and the temperature maximum is set to 280 °C and allowed to decrease to 240 °C between cycles. In Figure 1 with the cycled power graphic, the definition of cycle number is defined as it relates to the experimental data presented in Figure 4. The average temperature of the reaction is approximately 260 °C.

The overall MW power impingent of the samples is higher than that in the constant temperature mode (Supporting Information Figure SF5). For instance, an 8 cycle reaction requiring 4.5 min of reaction time has 38% higher MW power impingent on the reactants when compared to that in the reaction at a constant reaction temperature (280 °C) for the same reaction time.

At 0 cycle (Figure 4a), cube-shaped nanoparticles of ∼26 nm diameter are observed (size distribution provided in Supporting Information SF6). With increasing number of cycles (Figure 4B−F), anisotropic multipod structures are observed wherein the arm length and aspect ratio increase with the number of cycles. The isolated materials are fcc based on powder X-ray diffraction (Supporting Information Figure SF3).

DOI: 10.1021/acsnano.8b01992
ACS Nano 2018, 12, 6784−6793

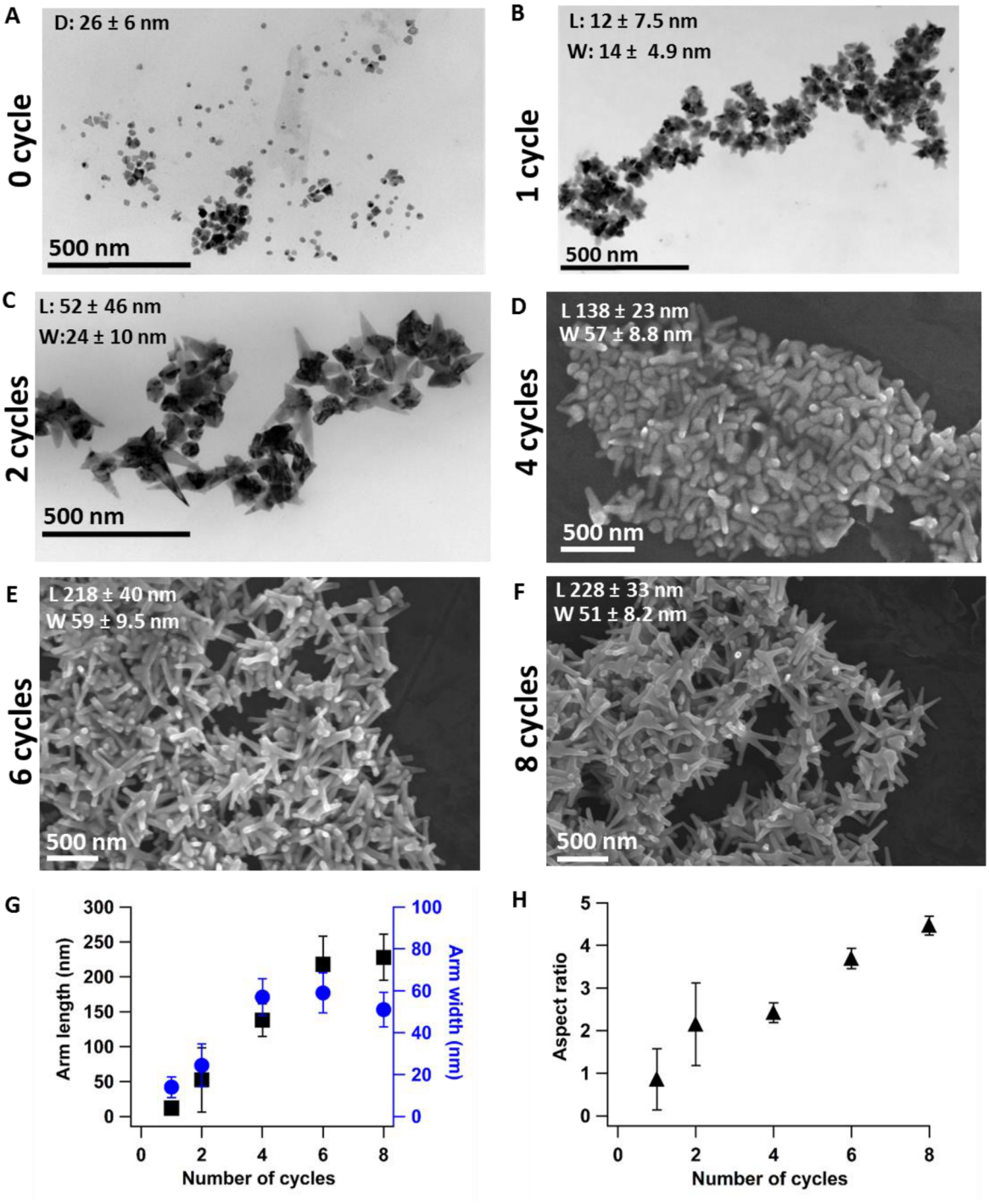

Figure 4. Evolution of the nickel multipod structure synthesized using cycled power mode with increasing number of cycles shown by TEM for (A) 0 cycle, (B) 1 cycle, (C) 2 cycles, (D) 4 cycles, (E) 6 cycles, and (F) 8 cycles. Insets in D and F show high-resolution TEM of the crystalline lattice of multipod arms. (G) Length and width of multipod arms as a function of the number applied after the initial cycle and (H) aspect ratio of arms *versus* number of cycles after the initial cycle.

A plot of the average length of the arms and widths, as well as the aspect ratio (length/width) as a function of the number of cycles, is plotted in Figure 4G,H. Analysis of the scanning electron microscopy (SEM) image for the 8 cycle reaction, in Figure 4 demonstrates >99% multipod formation (within 2σ) with an average of four arms per multipod. The distribution is a Gaussian distribution (Supporting Information SF7). The length of the arms is 228 ± 33 nm with a width of about 51 ± 8.2 nm, resulting in an aspect ratio of 4.5.

The multipod arms exhibit no glide plane errors and grow as (111) extensions. HRTEM imaging of the 4 cycle and 8 cycle sample reveals the arms are single crystal along the ⟨111⟩ direction with *d*-spacing of 0.20 nm (Supporting Information Figure SF2C,D). A HRTEM image of some initially formed Ni cores (0 cycle reaction) and a region near the core−arm interface for the 8 cycle reaction shows defect-free single-crystalline nature (Figure 5).

DOI: 10.1021/acsnano.8b01992
ACS Nano 2018, 12, 6784−6793

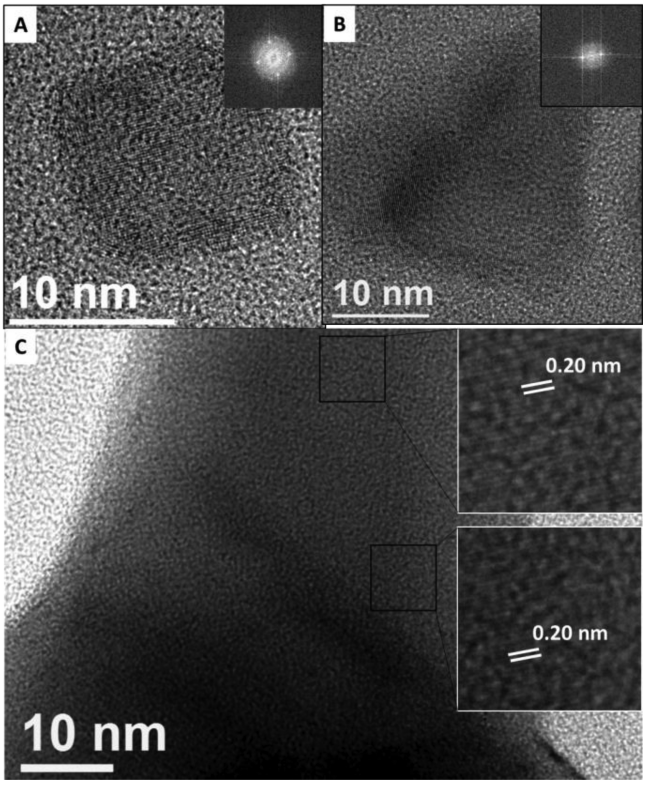

Figure 5. (A,B) High-resolution TEM images of core structures exhibiting single-crystalline nature without defect. (Insets) Numerical electron diffraction patterns corresponding to fast Fourier transform within the core region. (C) TEM of a multipod arm (8 cycle reaction) near the core−arm intersection, showing a highly crystalline defect-free structure as observed in magnified insets in two regions with a *d*-spacing of 0.20 nm corresponding to the (111) planes.

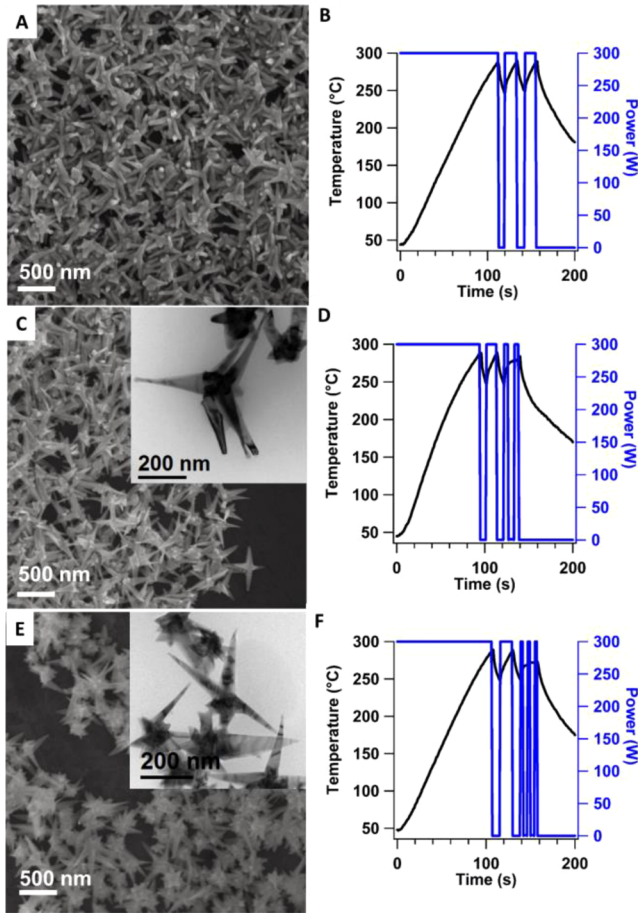

Figure 6. SEM of nanostructures with corresponding temperature and microwave power profile of cycled power reaction with different cycle frequencies following an initial cycle of 10 s at 300 W: (A,B) 1 cycle of 300 W for 10 s, (C,D) 2 cycles of 300 W for 5 s, and (E,F) 3 cycles of 300 W for 3 s. TEM image of multipod structure (insets of C and E).

The increase in the aspect ratio for the (111) arm is shown for the 10 s MW-on cycles in Figure 4H. The aspect ratio appears to be linear with respect to the number of cycles. The histograms for arm length and width are available in Supporting Information Figures SF7 and SF8. In Figure 6, the impact of shorter MW heating cycles is evaluated. Comparison of nearly equivalent heating times for a single 10 s cycle, two 5 s cycles, and three 3 s cycles following the initial 13 s MW irradiation event confirms the control of aspect ratio. The arm length and width can be extracted by analysis of 300 arms in the SEM images (Supporting Information Figure SF9). For the 10 s cycle (Figure 6A), the length is 178 ± 37.9 nm and the arm is 57.6 ± 7.87 nm (aspect ratio 3.1); for the two 5 s MW-on cycles (Figure 6B) the length is 246 ± 44.4 nm and the arm is 42.2 ± 10.1 nm (aspect ratio 5.8); and for the three 3 s MW-on cycles (Figure 6C), the length is 277 ± 49.6 nm and the arm is 41.1 ± 10.5 nm (aspect ratio 6.8). From the cycling study, it is clear that for the shorter MW-on cycle times, thinner arms are observed.

The resultant multipods in the cycled experiments compared to those in the constant temperature study reveal that under cycled power conditions the uniformity of the multipods is significantly better with a higher multipod density. The observed multipod density is in fact the highest ratio reported in the literature, with >99% for experimental conditions of four or more cycles. The observed experimental data are consistent with the overgrowth model for multipod formation suggested by Xia *et al.*[5]

Effect of Cycle Power on Multipod Evolution. Although it would be desirable to measure the tip *versus* core of the Ni multipod during the MW cycle to support the lightning rod mechanism, it is not practical to measure this on the scale of the nanoparticle. The MW measures vessel temperature and not the nanoparticle temperature directly. In order to support that growth behavior is dependent on MW-on cycling leading to tip heating, a series of experiments were carried out where the influence of MW power on the growth behavior was evaluated. It is reasonable to assume the higher cycle powers will lead to hotter tips, even though the average reaction temperature is nearly constant. However, the time to achieve temperature is lengthened at lower power, which should lead to nanoparticle temperature equilibration. (Note: For these reactions, a 10 mL reaction vessel was used which impacts the MW energy absorbed and the growth rates.)

As seen in Figure 7A,B, by lowering the power of the 4 cycle reaction to 150 W, the population of multipods is greatly reduced and primarily forms spherical nanoparticles (diameter = 52.4 ± 13.9 nm) in comparison to the 300 W 4 cycle reaction (Figure 7C,D), which produces well-defined multipods (arm length = 73.6 ± 27.1, arm width = 33.5 ± 5.6 nm).

DOI: 10.1021/acsnano.8b01992
ACS Nano 2018, 12, 6784−6793

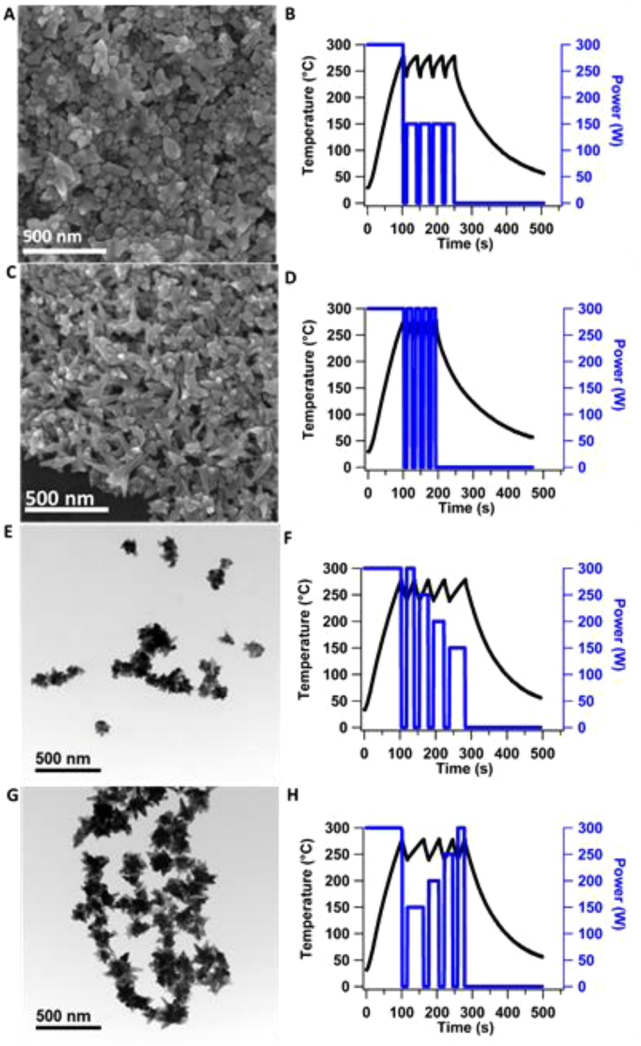

Figure 7. SEM of nanostructures with corresponding temperature and microwave power profile of reactions under cycled power of 150 W (A,B) and 300 W (C,D). TEM of nanostructures with corresponding temperature and microwave power profile of reactions under cycled power with sequential cycles of either decreasing power from 300 to 150 W (E,F) or increasing power from 150 to 300 W (G,H).

Furthermore, two other experiments were carried out where the sequential cycle power of the 4 cycles was either increased or decreased by 50 W. When the cycle power is sequentially decreased from 300 to 150 W in a 4 cycle reaction (Figure 7E,F), the nanostructures formed are more rounded with very little overgrowth (arm length = 22.2 ± 6.7 nm, arm width = 13.9 ± 3.4 nm). In the other case, where the MW power of sequential cycles is increased from 150 to 300 W (Figure 7G,H), multipods with longer arms are formed (arm length = 55.9 ± 18.5 nm, arm width = 28.0 ± 5.2 nm). Distribution of arm lengths and arm widths are provided in Supporting Information Figure SF10.

The power-dependent growth behavior can be ascribed to a lower temperature differential between the core and the tips when the cycle power is sequentially decreased, leading to more uniform nanoparticle surface heating and growth. On the other hand, when the cycle power is increased sequentially, the initially formed overgrowths continue to be selectively heated compared to the rest of the nanoparticle surface with subsequent high-power short-time cycles as described previously.

Role of Ligands on Multipod Generation under Constant Temperature and Cycled MW Power Modes. As a final check on the MW-on cycle-dependent growth, the influence of the ligand was investigated, as it is known ligands can direct nanoparticle shaping.[1,7,9,14] A set of experiments were carried out under both constant temperature (8 min) and cycled MW power (4 cycles of 300 W), where the ratio of the OAm (reducing agent and capping agent) and OAc (capping agent) was varied (Figure 8). In addition, we investigated the effect of nanoparticle growth when the primary amine (OAm) is substituted with a tertiary amine, trioctylamine (TOA).

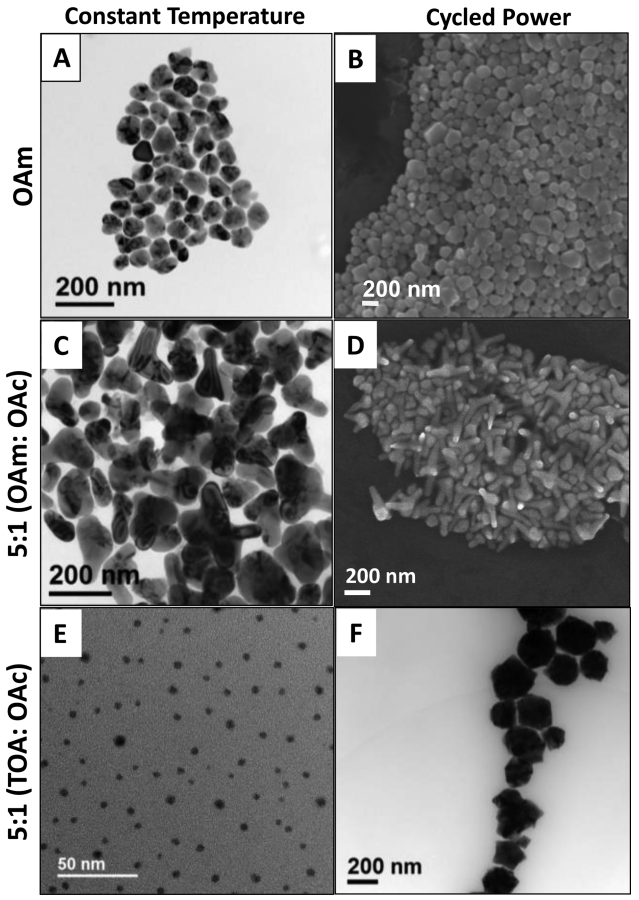

Figure 8. Ligand role in Ni multipod synthesis. Nanostructures formed using pure oleylamine (OAm) under (A) constant temperature mode for 10 min (TEM) and (B) cycled MW power with 12 cycles (SEM) (4 cycles did not form any product). Nanostructures formed using a 5:1 v/v ratio of OAm and oleic acid (OAc) under (C) constant temperature mode for 10 min (TEM) and (D) cycled MW power with 4 cycles (SEM). Nanostructures formed using a 5:1 v/v ratio of trioctylamine (TOA) to OAc under (E) constant temperature mode for 10 min (TEM) and (F) cycled MW power with 4 cycles (SEM). Reactions carried out using a 1:5 v/v ratio of OAm/OAc and using pure OAc yielded no product.

As shown in Figure 8C,D, reactions carried out at 5:1 OAm:OAc in the 10 mL reaction vessel produce multipod structures. The formation of the multipod is likely to be enhanced by the presence of OAc as the ligand-directing ability of OAc to enhance anisotropic shapes is well-documented. Reactions carried out at 1:5 or 0:1 OAm:OAc (not shown) do

DOI: 10.1021/acsnano.8b01992
ACS Nano 2018, 12, 6784–6793

not yield product due to too little reducing agent, consistent with the requirement of an amine to act as a reducing agent to initiate reduction of the $Ni(acac)_2$ to initiate Ni growth.[2,24] When the MW experiments (Figure 8A,B) are carried out at 1:0 OAm:OAc, spherical-shaped nanoparticles form, consistent with the requirement of OAc being present to direct nanoparticle shape. The isolated Ni spheres' constant temperature conditions have a diameter of 74.5 ± 13.0 nm, and following a reaction with 12 cycles at 300 W, the nanoparticle diameter is 137 ± 37 nm.

Interestingly, the Ni nanoparticles formed using a 5:1 v/v TOA:OAc ratio also eliminated multipod growth under constant temperature and cycled MW power modes. Under constant temperature mode, spherical nanoparticles with a diameter of 4.63 ± 1.62 nm were isolated, whereas the cycled MW power mode produced large faceted nanoparticles with diameters of 173 ± 70 nm. The difference in growth is not understood but is under study. We believe the loss of the multipod structure reflects loss of packing order at the surface due to the presence of bound TOA.

The observation from the ligand studies suggests that the combination of OAm and OAc is key to the formation of a Ni core structure with overgrowths that can then be elongated most effectively through MW power cycling. Further studies are underway to explore the full role of the ligand.

Analysis of the Magnetic and Thermal Stability Properties of Ni Multipods. The multipod structures with high anisotropic structures may have applications in a range of technical fields, including magnetism and catalysis. The magnetic characterization and thermal stability of selected multipods were analyzed for completeness. The data are provided in Supporting Information Figures SF11 and SF12.

It is known that shape anisotropy in magnetic materials is known to influence the magnetic properties of materials.[49,50] Results from the magnetic field-sweep studies carried out at 300 K show that the anisotropic nature of the multipod arms influences the coercivity of the materials while maintaining a high saturation magnetization value (Supporting Information Figure SF11). The coercivity increases from 215 Oe (arm aspect ratio of 2.17) to 250 Oe (arm aspect ratio of 2.42) and finally 283 Oe (arm aspect ratio of 4.47) as the aspect ratio of the multipod arms increases. In comparison, spherical Ni fcc nanoparticles of 55 nm diameter we have synthesized exhibit a coercivity of only 109 Oe at 300 K. The values of coercivity at 300 K for Ni multipods from the 8 cycle reaction are greater than that of many of the Ni nanostructures synthesized to date.[18,51−54]

Catalytic reactions are often carried out at high temperature, and the benefits of high surface area multipods are only applicable if the structures are stable. In order to probe the structural stability of the multipods at higher temperatures, which are typically used for catalytic studies, a series of experiments were carried out where the multipod structures from the 300 W 8 cycle reaction were thermally heated at 200, 400, and 600 °C for 30 min in a thermogravimetric analysis (TGA) instrument and imaged by SEM post-treatment. The SEM images for the multipods pre- and post-thermal treatment show that the multipod morphology is maintained even at 400 °C without any observation of reconstruction to spherical morphology (Supporting Information Figure SF12). At 600 °C, the particles start to fuse with each other as ligand loss has taken place, and melting alongside surface reconstruction of the multipods seems to occur at this temperature.

CONCLUSION

Size-tunable nickel multipod structures were synthesized using a cycled microwave heating approach that provided greater control over growth and produces good quality metallic nickel nanostructures with tight size distributions. Particle analysis by pXRD and TEM reveal pure fcc phase Ni structures with arms that grow along the ⟨111⟩ direction. The experimental results support that proposed anisotropic growth control is due to the MW power cycling of the microwave field as suggested in the proposed mechanism in Figure 1. Results from this work suggest a temperature difference between the multipod tips *versus* the rest of the nanoparticle achieved through selective heating of the tips during the "on" step of the reaction enables the arms to grow rapidly along the tip. During the power "on" step of the microwave, the tips of the multipods heat rapidly in comparison to the other parts of the nanoparticle owing to the lightning rod effect.[25−33] Selective heating of (111) tips leads to an increase in the surface-mediated autocatalytic growth at the tip, leading to the observed multipod structures. High-power cycles provide greater differential temperature, which impacts arm growth more significantly than total reaction time or average reaction temperature. From the tapering of the multipod width from the base to the tip and single-crystalline nature of the arms, the nanoparticle growth cannot be ascribed to oriented attachment of smaller nanoparticles formed at the initial stages of the reaction.

The use of MW power cycles to control multipod structures is advantageous as the synthesis approach uses only three reactants and can be carried out under ambient conditions within minutes. Synthesis times for even the largest multipods took less than 15 min with the cycled microwave approach. This cycled heating approach should apply to other material types and further illustrates the important role of microwave−matter interactions in the synthesis of materials using microwave-based heating. The catalytic properties of such highly branched structures with different arm sizes is currently being investigated.

EXPERIMENTAL SECTION

Materials. Nickel acetylacetonate hydrate ($Ni(acac)_2{\cdot}xH_2O$, 99%), oleic acid (OAc), oleylamine (OAm, technical grade 70%), tri-*n*-octylamine (TOA), toluene, methanol (MeOH), acetone, and chloroform were purchased from Sigma-Aldrich. The materials were used without further purification.

Synthesis of Nanoparticles. *Microwave Synthesis of Nickel Multipods.* Ni multipods were prepared by MW heating a solution containing 0.75 mmol of nickel acetylacetonate, 25 mmol of OAm (or TOA), and 5 mmol of OA. The reaction was performed in a 2.45 GHz single-mode Anton-Paar Monowave 300 microwave using a G30 (30 mL) Anton-Paar microwave vessel that was sealed with a silicone septa and crimp cap. The blue reaction solution was degassed under vacuum with stirring at a temperature of approximately 100 °C for 30 min using a water bath until no more bubbling was observed prior to MW heating (note: this step is not required but carried out as standard protocol). The nanoparticles were grown by heating the reaction to 280 °C using 300 W of microwave power followed by one of three operational modes: (1) constant temperature mode (280 °C) (instrument maintains temperature by adjusting the microwave power automatically) for a fixed duration of time, (2) a custom profile where the microwave power is stepped to a lower constant power value that can maintain the temperature at an almost constant value, or (3) a custom profile where the instrument is programmed to deliver microwave power in an on/off cyclic manner. During the cycling mode, the microwave power is completely off while the reaction cools from 280 to 240 °C (10 s using automatic forced air) between the

DOI: 10.1021/acsnano.8b01992
ACS Nano 2018, 12, 6784−6793

"on" cycles where the microwave delivers a fixed amount of power to increase the temperature back to 280 °C, as illustrated by the power–temperature reaction profiles in the figures within the paper for the various reactions. The time to increase the temperature from 240 to 280 °C depends on the selected power (300 W, 13 s; 150 W, 26 s). For cycled 300 W power reactions with different frequencies (2 cycles of 5 s or 3 cycles of 3 s), the power between cycles is reduced to 1 W instead of air cooling as the microwave system cannot respond on such short time scales without lowering the reaction temperature significantly. Following the last "on" cycle, the solution is cooled to 55 °C and the nanoparticles are isolated by magnetic separation, followed by three repeat toluene dissolutions, methanol precipitation, magnetic isolation, and finally drying the particles under vacuum.

In the case of smaller particles that do not separate out magnetically, the nickel nanoparticles were precipitated by addition of 5 mL of toluene followed by 15 mL of methanol. The resulting solution was centrifuged for 5 min using a centrifuge tube. After the supernatant was removed, the pellet was redispersed in toluene. To precipitate the NiNPs, excess methanol was added followed by isolation through centrifugation before being dried under vacuum.

Synthesis of Nickel Nanoparticles by Convective Heating. Convectively prepared Ni nanoparticles were prepared using the same reaction solution in a microwave glass vessel (Anton-Paar G30) heated to 280 °C from room temperature (4 °C/min) and held at 280 °C for 1 h using a heating mantle after prior degassing under vacuum at 100 °C for 30 min (the reaction was opened to air). A second reaction was also carried out where the reaction vessel was placed in a preheated aluminum block at 280 °C to increase the heating rate to closely match that of the initial ramp in the microwave. The reactions were cooled quickly to room temperature using a blower, and the nanoparticles were cleaned as described previously.

Transmission Electron Microscopy. Nanoparticle samples were drop-cast from a toluene dispersion onto 300 mesh carbon-coated copper grids and left to dry under vacuum overnight. The TEM images were recorded using a JEM-ARM200cF electron microscope at 200 kV acceleration voltage.

Scanning Electron Microscopy. SEM imaging was performed on aluminum mounts with nanoparticles drop-casted directly and allowed to dry. SEM imaging was performed on a FEI Nova NanoSEM 400 operating at 20 kV with a spot size of 4.0. The images were collected with an Everhart-Thornley detector.

Powder X-ray Diffraction. The pXRD patterns for Ni nanoparticles were acquired on a Rigaku Ultima III diffractometer equipped with a Cu Kα source. Data wre collected at room temperature in the 2θ range of 10–84°.

Magnetic Measurements. Magnetic properties were studied with a superconducting quantum interference device (SQUID) magnetometer, MPMS-XL (Quantum Design). Field-dependent magnetization for nanostructures embedded in paraffin wax was measured at 300 K, with the applied field varying from 0 to 1.5 T and back.

Thermogravimetric Analysis. TGA was performed on a TA Instruments Q50 thermogravimetric analyzer. The samples were heated at a rate of 10 °C/min from room temperature to 100 °C in an alumina pan and held for 5 min before continuing to ramp at 10 °C/min to the final temperature (200–600 °C). The samples were held at the final temperature for 30 min. Measurements were performed under nitrogen environment.

ASSOCIATED CONTENT

Supporting Information

The Supporting Information is available free of charge on the ACS Publications website at DOI: 10.1021/acsnano.8b01992.

Additional pXRD, HRTEM, SEM, SQUID, TGA, and particle size analysis data (PDF)

AUTHOR INFORMATION

Corresponding Author

*E-mail: strouse@chem.fsu.edu

ORCID

Geoffrey F. Strouse: 0000-0003-0841-282X

Author Contributions

P.N.V. prepared the samples, characterized the samples, assisted in the interpretation and writing of the manuscript. D.A.H. characterized samples by SEM and assisted in analysis of SEM data. G.F.S. designed the project, assisted in interpretation and conclusions and in the writing of the manuscript. All authors revised the manuscript.

Notes

The authors declare no competing financial interest.

ACKNOWLEDGMENTS

G.F.S., P.N.V., and D.A.H. wish to thank the National Science Foundation (NSF CHE-1608364) for funding. The TEM imaging at FSU is supported by the Florida State University Research Foundation and through the National High Magnetic Field Laboratory National Science Foundation Cooperative Agreement DMR-1157490 and 1644779, the State of Florida, and Florida State University.

REFERENCES

(1) Yin, X.; Shi, M.; Wu, J.; Pan, Y.-T.; Gray, D. L.; Bertke, J. A.; Yang, H. Quantitative Analysis of Different Formation Modes of Platinum Nanocrystals Controlled by Ligand Chemistry. *Nano Lett.* **2017**, *17*, 6146–6150.

(2) Ashley, B.; Vakil, P. N.; Lynch, B. B.; Dyer, C. M.; Tracy, J. B.; Owens, J.; Strouse, G. F. Microwave Enhancement of Autocatalytic Growth of Nanometals. *ACS Nano* **2017**, *11*, 9957–9967.

(3) Yang, T.-H.; Zhou, S.; Gilroy, K. D.; Figueroa-Cosme, L.; Lee, Y.-H.; Wu, J.-M.; Xia, Y. Autocatalytic Surface Reduction and Its Role in Controlling Seed-Mediated Growth of Colloidal Metal Nanocrystals. *Proc. Natl. Acad. Sci. U. S. A.* **2017**, *114*, 13619.

(4) Alyami, N. M.; LaGrow, A. P.; Anjum, D. H.; Guan, C.; Miao, X.-H.; Sinatra, L.; Yuan, D.-J.; Mohammed, O. F.; Huang, K.-W.; Bakr, O. M. Synthesis and Characterization of Branched Fcc/Hcp Ruthenium Nanostructures and Their Catalytic Activity in Ammonia Borane Hydrolysis. *Cryst. Growth Des.* **2018**, *18*, 1509.

(5) Jin, M.; Zhang, H.; Xie, Z.; Xia, Y. Palladium Concave Nanocubes with High-Index Facets and Their Enhanced Catalytic Properties. *Angew. Chem., Int. Ed.* **2011**, *50*, 7850–7854.

(6) Wang, H.; Yin, S.; Li, Y.; Yu, H.; Li, C.; Deng, K.; Xu, Y.; Li, X.; Xue, H.; Wang, L. One-Step Fabrication of Tri-metallic PdCuAu Nanothorn Assemblies as an Efficient Catalyst for Oxygen Reduction Reaction. *J. Mater. Chem. A* **2018**.

(7) Watt, J.; Cheong, S.; Tilley, R. D. How to Control the Shape of Metal Nanostructures in Organic Solution Phase Synthesis for Plasmonics and Catalysis. *Nano Today* **2013**, *8*, 198–215.

(8) He, R.; Wang, Y.-C.; Wang, X.; Wang, Z.; Liu, G.; Zhou, W.; Wen, L.; Li, Q.; Wang, X.; Chen, X.; Zeng, J.; Hou, J. G. Facile Synthesis of Pentacle Gold–copper Alloy Nanocrystals and Their Plasmonic and Catalytic Properties. *Nat. Commun.* **2014**, *5*, 4327.

(9) Zhang, J.; Kuang, Q.; Jiang, Y.; Xie, Z. Engineering High-Energy Surfaces of Noble Metal Nanocrystals with Enhanced Catalytic Performances. *Nano Today* **2016**, *11*, 661–677.

(10) Strasser, P.; Gliech, M.; Kuehl, S.; Moeller, T. Electrochemical Processes on Solid Shaped Nanoparticles with Defined Facets. *Chem. Soc. Rev.* **2018**, *47*, 715.

(11) Luo, S.; Shen, P. K. Concave Platinum–Copper Octopod Nanoframes Bounded with Multiple High-Index Facets for Efficient Electrooxidation Catalysis. *ACS Nano* **2017**, *11*, 11946–11953.

(12) Ye, E.; Regulacio, M. D.; Zhang, S.-Y.; Loh, X. J.; Han, M.-Y. Anisotropically Branched Metal Nanostructures. *Chem. Soc. Rev.* **2015**, *44*, 6001–6017.

(13) Cao, Z.; Chen, Q.; Zhang, J.; Li, H.; Jiang, Y.; Shen, S.; Fu, G.; Lu, B.; Xie, Z.; Zheng, L. Platinum-Nickel Alloy Excavated Nano-

DOI: 10.1021/acsnano.8b01992
ACS Nano 2018, 12, 6784–6793

Multipods with Hexagonal Close-Packed Structure and Superior Activity towards Hydrogen Evolution Reaction. *Nat. Commun.* **2017**, *8*, 15131.
(14) Xia, Y.; Xiong, Y.; Lim, B.; Skrabalak, S. E. Shape-controlled Synthesis of Metal Nanocrystals: Simple Chemistry Meets Complex Physics? *Angew. Chem., Int. Ed.* **2009**, *48*, 60−103.
(15) Weiner, R. G.; DeSantis, C. J.; Cardoso, M. B. T.; Skrabalak, S. E. Diffusion and Seed Shape: Intertwined Parameters in the Synthesis of Branched Metal Nanostructures. *ACS Nano* **2014**, *8*, 8625−8635.
(16) Watt, J.; Cheong, S.; Toney, M. F.; Ingham, B.; Cookson, J.; Bishop, P. T.; Tilley, R. D. Ultrafast Growth of Highly Branched Palladium Nanostructures for Catalysis. *ACS Nano* **2010**, *4*, 396−402.
(17) Teng, X.; Yang, H. Synthesis of Platinum Multipods: An Induced Anisotropic Growth. *Nano Lett.* **2005**, *5*, 885−891.
(18) Shviro, M.; Zitoun, D. Nickel Nanocrystals: Fast Synthesis of Cubes, Pyramids and Tetrapods. *RSC Adv.* **2013**, *3*, 1380−1387.
(19) Su, N.; Chen, X.; Yue, B.; He, H. Formation of Palladium Concave Nanocrystals *via* Auto-Catalytic Tip Overgrowth by Interplay of Reduction Kinetics, Concentration Gradient and Surface Diffusion. *Nanoscale* **2016**, *8*, 8673−8680.
(20) LaGrow, A. P.; Cheong, S.; Watt, J.; Ingham, B.; Toney, M. F.; Jefferson, D. A.; Tilley, R. D. Can Polymorphism Be Used to Form Branched Metal Nanostructures? *Adv. Mater.* **2013**, *25*, 1552−1556.
(21) Lim, B.; Xia, Y. Metal Nanocrystals with Highly Branched Morphologies. *Angew. Chem., Int. Ed.* **2011**, *50*, 76−85.
(22) Kunal, P.; Roberts, E. J.; Riche, C. T.; Jarvis, K.; Malmstadt, N.; Brutchey, R. L.; Humphrey, S. M. Continuous Flow Synthesis of Rh and RhAg Alloy Nanoparticle Catalysts Enables Scalable Production and Improved Morphological Control. *Chem. Mater.* **2017**, *29*, 4341−4350.
(23) Dahal, N.; García, S.; Zhou, J.; Humphrey, S. M. Beneficial Effects of Microwave-Assisted Heating versus Conventional Heating in Noble Metal Nanoparticle Synthesis. *ACS Nano* **2012**, *6*, 9433−9446.
(24) Ashley, B.; Dyer, C. M.; Owens, J.; Strouse, G. F. Influence of Microwave Frequency and Power on Nanometal Growth. *J. Phys. Chem. C* **2018**, *122*, 3617.
(25) Cobley, C. M.; Skrabalak, S. E.; Campbell, D. J.; Xia, Y. Shape-Controlled Synthesis of Silver Nanoparticles for Plasmonic and Sensing Applications. *Plasmonics* **2009**, *4*, 171−179.
(26) Sun, J.; Wang, W.; Yue, Q. Review on Microwave-Matter Interaction Fundamentals and Efficient Microwave-Associated Heating Strategies. *Materials* **2016**, *9*, 231.
(27) Rajeev, P. P.; Ayyub, P.; Bagchi, S.; Kumar, G. R. Nanostructures, Local Fields, and Enhanced Absorption in Intense Light−matter Interaction. *Opt. Lett.* **2004**, *29*, 2662−2664.
(28) Zhuo, R. F.; Qiao, L.; Feng, H. T.; Chen, J. T.; Yan, D.; Wu, Z. G.; Yan, P. X. Microwave Absorption Properties and the Isotropic Antenna Mechanism of ZnO Nanotrees. *J. Appl. Phys.* **2008**, *104*, 094101.
(29) Liao, P. F.; Wokaun, A. Lightning Rod Effect in Surface Enhanced Raman Scattering. *J. Chem. Phys.* **1982**, *76*, 751−752.
(30) Li, Y.; Xu, F.; Hu, X.; Luan, Y.; Han, Z.; Wang, Z. Focusing Effect of Electromagnetic Fields and Its Influence on Sintering during the Microwave Processing of Metallic Particles. *J. Mater. Res.* **2015**, *30*, 3663−3670.
(31) Hongtao, Z.; Xijiang, H.; Lifang, Z.; Gangyi, W.; Chao, W.; Xueai, L.; Ping, X. Controlled Synthesis and Morphology-Dependent Electromagnetic Properties of Nickel Nanostructures by γ-Ray Irradiation Technique. *Radiat. Phys. Chem.* **2011**, *80*, 390−393.
(32) Sajanlal, P. R.; Sreeprasad, T. S.; Samal, A. K.; Pradeep, T. Anisotropic Nanomaterials: Structure, Growth, Assembly, and Functions. *Nano Rev.* **2011**, *2*, 5883.
(33) Liu, Q.; Xu, X.; Xia, W.; Che, R.; Chen, C.; Cao, Q.; He, J. Dependency of Magnetic Microwave Absorption on Surface Architecture of Co20Ni80 Hierarchical Structures Studied by Electron Holography. *Nanoscale* **2015**, *7*, 1736−1743.
(34) Wang, C.; Han, X.; Xu, P.; Wang, J.; Du, Y.; Wang, X.; Qin, W.; Zhang, T. Controlled Synthesis of Hierarchical Nickel and Morphology-Dependent Electromagnetic Properties. *J. Phys. Chem. C* **2010**, *114*, 3196−3203.
(35) Wang, C.; Hu, S.; Han, X.; Huang, W.; Tian, L. Controlled Synthesis and Microwave Absorption Property of Chain-Like Co Flower. *PLoS One* **2013**, *8*, e55928.
(36) An, Z.; Pan, S.; Zhang, J. Synthesis and Tunable Assembly of Spear-like Nickel Nanocrystallites: From Urchin-like Particles to Prickly Chains. *J. Phys. Chem. C* **2009**, *113*, 1346−1351.
(37) Imran Din, M.; Rani, A. Recent Advances in the Synthesis and Stabilization of Nickel and Nickel Oxide Nanoparticles: A Green Adeptness. *Int. J. Anal. Chem.* **2016**, *2016*, 3512145.
(38) Tasker, S. Z.; Standley, E. A.; Jamison, T. F. Recent Advances in Homogeneous Nickel Catalysis. *Nature* **2014**, *509*, 299.
(39) Alonso, F.; Riente, P.; Yus, M. Nickel Nanoparticles in Hydrogen Transfer Reactions. *Acc. Chem. Res.* **2011**, *44*, 379−391.
(40) Polshettiwar, V.; Baruwati, B.; Varma, R. S. Nanoparticle-Supported and Magnetically Recoverable Nickel Catalyst: A Robust and Economic Hydrogenation and Transfer Hydrogenation Protocol. *Green Chem.* **2009**, *11*, 127−131.
(41) Carenco, S.; Boissière, C.; Nicole, L.; Sanchez, C.; Le Floch, P.; Mézailles, N. Controlled Design of Size-Tunable Monodisperse Nickel Nanoparticles. *Chem. Mater.* **2010**, *22*, 1340−1349.
(42) Zhu, Y.-J.; Chen, F. Microwave-Assisted Preparation of Inorganic Nanostructures in Liquid Phase. *Chem. Rev.* **2014**, *114*, 6462−6555.
(43) Zhi, C.; Dai, M.; Yuji, W. Precisely Controlled Synthesis of Metal Nanoparticles under Microwave Irradiation. *Microwaves in Nanoparticle Synthesis*; Wiley-Blackwell, 2013; pp 145−183.
(44) Kitchen, H. J.; Vallance, S. R.; Kennedy, J. L.; Tapia-Ruiz, N.; Carassiti, L.; Harrison, A.; Whittaker, A. G.; Drysdale, T. D.; Kingman, S. W.; Gregory, D. H. Modern Microwave Methods in Solid-State Inorganic Materials Chemistry: From Fundamentals to Manufacturing. *Chem. Rev.* **2014**, *114*, 1170−1206.
(45) Mourdikoudis, S.; Collière, V.; Amiens, C.; Fau, P.; Kahn, M. L. Metal−Organic Pathways for Anisotropic Growth of a Highly Symmetrical Crystal Structure: Example of the Fcc Ni. *Langmuir* **2013**, *29*, 13491−13501.
(46) Ma, F.; Ma, J.; Huang, J.; Li, J. The Shape Dependence of Magnetic and Microwave Properties for Ni Nanoparticles. *J. Magn. Magn. Mater.* **2012**, *324*, 205−209.
(47) Hoefelmeyer, J. D.; Niesz, K.; Somorjai, G. A.; Tilley, T. D. Radial Anisotropic Growth of Rhodium Nanoparticles. *Nano Lett.* **2005**, *5*, 435−438.
(48) Cozzoli, P. D.; Snoeck, E.; Garcia, M. A.; Giannini, C.; Guagliardi, A.; Cervellino, A.; Gozzo, F.; Hernando, A.; Achterhold, K.; Ciobanu, N.; Parak, F. G.; Cingolani, R.; Manna, L. Colloidal Synthesis and Characterization of Tetrapod-Shaped Magnetic Nanocrystals. *Nano Lett.* **2006**, *6*, 1966−1972.
(49) Song, Q.; Zhang, Z. J. Shape Control and Associated Magnetic Properties of Spinel Cobalt Ferrite Nanocrystals. *J. Am. Chem. Soc.* **2004**, *126*, 6164−6168.
(50) Hyeon, T. Chemical Synthesis of Magnetic Nanoparticles. *Chem. Commun.* **2003**, 927−934.
(51) Donegan, K. P.; Godsell, J. F.; Tobin, J. M.; O'Byrne, J. P.; Otway, D. J.; Morris, M. A.; Roy, S.; Holmes, J. D. Microwave-Assisted Synthesis of Icosahedral Nickel Nanocrystals. *CrystEngComm* **2011**, *13*, 2023−2028.
(52) Li, P.; Wang, N.; Wang, R. Flower-Like Nickel Nanocrystals: Facile Synthesis, Shape Evolution, and Their Magnetic Properties. *Eur. J. Inorg. Chem.* **2010**, *2010*, 2261−2265.
(53) Hu, X.; Yu, J. C. High-Yield Synthesis of Nickel and Nickel Phosphide Nanowires *via* Microwave-Assisted Processes. *Chem. Mater.* **2008**, *20*, 6743−6749.
(54) He, X.; Zhong, W.; Au, C.-T.; Du, Y. Size Dependence of the Magnetic Properties of Ni Nanoparticles Prepared by Thermal Decomposition Method. *Nanoscale Res. Lett.* **2013**, *8*, 446.

DOI: 10.1021/acsnano.8b01992
ACS Nano 2018, 12, 6784−6793